RSC Advances

PAPER

View Article Online
View Journal | View Issue

Cite this: *RSC Adv.*, 2015, **5**, 21206

$H_6P_2W_{18}O_{62}$/Nanoclinoptilolite as an efficient nanohybrid catalyst in the cyclotrimerization of aryl methyl ketones under solvent-free conditions

R. Tayebee* and M. Jarrahi

Received 23rd January 2015
Accepted 17th February 2015

DOI: 10.1039/c5ra01344e

www.rsc.org/advances

A new type of nanohybrid material $H_6P_2W_{18}O_{62}$/nanoclinoptilolite was fabricated and performed as an efficient and reusable catalyst in the mild and one-pot condensation of different acetophenones. The operational simplicity, easy work-up, cost-effective, and solvent-free nature of the present methodology were accompanied with good to excellent yields of the desired 1,3,5-triarylbenzenes from a wide range of alkyl, aryl, and cyclic ketones. The nanocatalyst was prepared *via* immobilization of *Wells–Dawson* heteropolyacid $H_6P_2W_{18}O_{62}$ (HPA) on the surface of nanoclinoptilolite (NCP). The nanohybrid material was easily recovered and reused successfully at least seven times without significant loss of catalytic activity. XRD, SEM, UV-Vis, MS-ICP, DTA, and FT-IR studies confirmed that the heteropolyacid is well dispersed on the surface of NCP. This protocol developed is a safe and convenient alternate method for the synthesis of 1,3,5-triarylbenzenes utilizing an eco-friendly and a highly reusable natural nanocatalyst. Furthermore, water was the only by-product, which made the present methodology environmentally benign.

1. Introduction

Screening environmentally benign methods for chemical syntheses is an important challenging and necessary subject to avoid the adverse consequences of usual chemical industries. Green chemical processes comprise application of sustainable and clean ways, using cost effective catalysts, employing water as solvent or exploitation of solvent-free systems. The present report introduces a new green route for the preparation of 1,3,5-triarylbenzenes. These compounds are important polycyclic aromatic hydrocarbons which have a uniform amorphous phase due to their molecular shapes and have exhibited potential applications for fabricating electrode and electroluminescent devices,[1] organic light emitting diodes, nanomaterials,[2] photovoltaic resisting materials, and conducting polymers.[3] Moreover, 1,3,5-triarylbenzenes are known as important intermediates in the synthesis of pharmaceuticals, fullerene fragments,[4] synthetic dendrimers,[5] and various conjugated polyaromatics.[6] These important compounds have been made by condensation of aryl methyl ketones in various acidic media *via* a number of synthetic procedures. Common *Brønsted* acids, *para*-toluene sulfonic acid, $Bi(OTf)_3$, $FeCl_3$, and *Amberlyst*-15 are widely handled for the preparation of triarylbenzenes.[7] Although these methods have proved to be useful, however, there are some limitations, including low yields, tedious workup, long reaction times, moisture sensitivity, specialized handling, non-recyclability of the catalyst, and using stoichiometric amounts of expensive and toxic catalysts.

Heteropolyacids constitute an extensive class of inorganic metal-oxo clusters comprising early transition metals in their highest oxidation state which show a great deal of applications in catalysis, material sciences, pharmaceuticals, and biology. *Wells–Dawson* heteropolyacid with the general formula of $[(X^{n+})_2M_{18}O_{62}]^{(16-2n)-}H^{(16-2n)+}$ is an important subclass of heteropolyacids. In this structure, X^{n+} represents a central atom such as, phosphorous(v), arsenic(v), sulfur(vi), fluorine; surrounded by a cage of M addenda atoms, such as tungsten(vi),molybdenum(vi) or a mixture of elements, each of them composing of MO_6 (M-oxygen) octahedral units. One of the most important disadvantages of this heteropolyacid lies in high solubility in polar media which causes separation problems. To overcome this limitation, it can be supported on different weak-acidic or non-basic carriers or immobilized on positively charged nanoparticles through covalent or electrostatic attractions. Up to now, several supports such as silica,[8] active carbon,[9] MCM-41,[10] SBA-15,[11] have been utilized to heterogenize heteropolyacids *via* immobilization. NCP as porous material could be used as a good candidate to accommodate and deposit heteropolyacids and produce effective catalysts in organic synthesis by consideration of either *Lewis* or *Brønsted* acidic characteristics of them.[12]

Herein, the capability of a new nanohybrid material HPA/NCP is assessed in the catalytic cyclotrimerization of 1,3,5-triarylbenzenes under solvent-free conditions (Scheme 1).

Department of Chemistry, School of Sciences, Hakim Sabzevari University, Sabzevar, 96179-76487, Iran. E-mail: Rtayebee@hsu.ac.ir; Fax: +98-51-44410300; Tel: +98-51-44410310

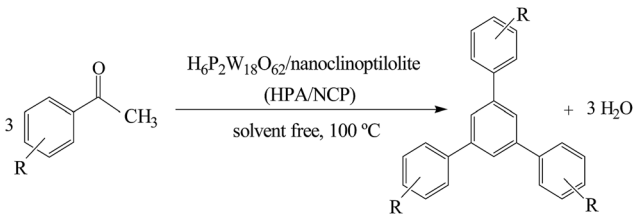

Scheme 1 General formulation for the cyclotrimerization of acetophenones.

2. Experimental

2.1. Materials and methods

All reagents and starting materials were commercially available and were used as received. Natural clinoptilolite-rich tuffs were obtained from *Sabzevar* region in the north-east of *Iran*. All solutions were prepared in double-distilled deionized water. Ball milling of the natural CP zeolite was carried out by means of a laboratory fast mill (Model 20436, Sanatceram, Iran) and a planetary ball mill (PM100; Retsch Corporation). Progress of the reactions was monitored by TLC on silica gel polygram SIL G/UV 254 plates. Melting points were recorded on a Bamstead electrothermal type 9200 melting point apparatus. Differential thermal analysis was carried out on a Netzch Germany, E404 analyzer instrument in air at a heating rate of 10 °C min^{-1}. Scanning electron microscope (SEM) micrographs were taken using a KYKY-EM3200 microscope (acceleration voltage 26 kV). Fourier transform infrared (FT-IR) spectra were recorded on a 8700 Shimadzu Fourier-Transform spectrophotometer in the region of 400 to 4000 cm^{-1} using KBr pellets. Ultraviolet-visible spectra were recorded on a Photonix UV-Vis Array spectrophotometer, Model Ar 2015, Iran. X-ray powder diffraction (XRD) analysis were performed on a XPert MPD diffractometer with Cu K_α radiation ($\lambda = 1.5406$) at 40 keV and 30 mA with a scanning rate of 3° min^{-1} in the 2θ range from 5° to 80°. ^1H and ^{13}C NMR spectra were recorded on a Bruker AVANCE 300 MHz instrument using TMS as internal reference. Tungsten content in the nanohybrid catalyst was determined using Inductivity Coupled Plasma-Mass Spectrometry (ICP-MS) conducted on a Perkin Elmer, Elan 6000 DRC ICP-MS spectrometer. All products were identified by comparison of their spectral and physical data with those previously reported.[13] *Wells–Dawson* diphosphooctadecatungstic acid $H_6P_2W_{18}O_{62}\cdot 24H_2O$ was prepared according to the literature method.[14]

2.2. Preparation of the NCP zeolite

The nanosized CP was obtained by means of a planetary ball mill in the dry state. In most of the experiments a clinoptilolite (CP) powder with the average particles size of 70 μm was applied as the starting material. Planetary ball milling was performed in dry conditions with a period of 60 min, 10 balls of 20 mm per 30 g of powder and a milling speed of 350 rpm. The experiments were performed in a 250 ml stainless steel jar with a protective jacket of zirconium oxide. Zirconium oxide balls were utilized for dry milling.[15]

2.3. Surface modification of NCP with the Wells–Dawson $H_6P_2W_{18}O_{62}\cdot 24H_2O$

For this purpose, five grams of the NCP (calcined at 650 °C for 4 h) was placed in contact with 100 ml of an aqueous solution of NH_4NO_3 (1 M). After shaking at 75 °C for 6 h in a thermostatic bath, the sample was separated by filtration, rinsed with deionized water, dried at 110 °C for 8 h, and calcined at 540 °C for 4 h. The obtained sample was again processed by a second acid treatment as mentioned above. To prepare the surface modified NCP, 0.1 g of $H_6P_2W_{18}O_{62}\cdot 24H_2O$ was dissolved in 40 ml of H_2O; then, 0.5 g of NCP was dispersed in the solution and the mixture was shaken at 70 °C for 4 h in a thermostatic bath. Finally, the sample was separated by filtration, rinsed with deionized water, and dried at 80 °C overnight.

2.4. General procedure for the conversion of acetophenone into 1,3,5-triphenylbenzene

In a typical reaction, acetophenone (1 mmol) and the surface modified NCP (15 mg) were added to a small test tube and the reaction mixture was stirred for 2.5 h at 100 °C. After completion of reaction, as indicated by TLC, the reaction mass was cooled to 25 °C; then, hot ethanol was added to the reaction mixture and the mixture was stirred for 5 min. The insoluble catalyst was isolated *via* simple filtration. The filtrate containing water as the only by-product of the cyclotrimerization, was concentrated

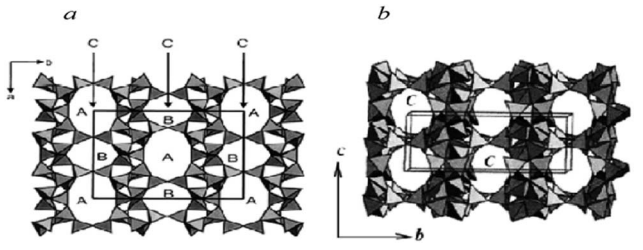

Fig. 1 Tetrahedral model of clinoptilolite, indicating 10-membered A and 8-membered B channels that are bridged with 8-membered C channels (projection along *c* axis) (a) and parallel channel C formed with the ellipsoidal 8-membered rings (b).[18]

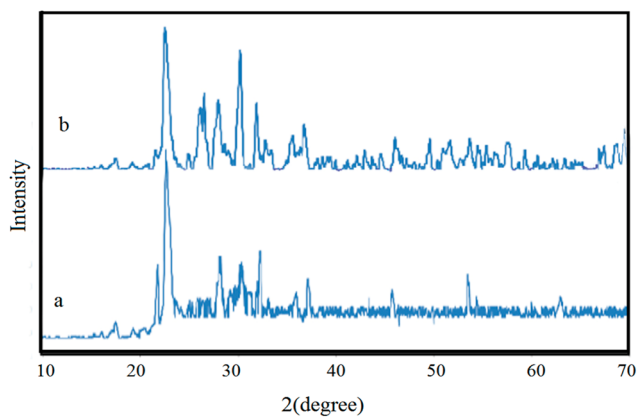

Fig. 2 XRD patterns of NCP (a) and $H_6P_2W_{18}O_{62}$/NCP (b).

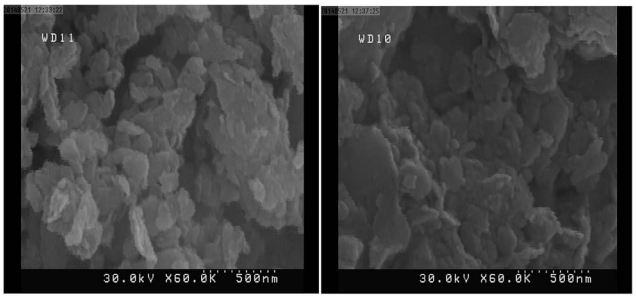

(a) (b)

Fig. 3 Representative SEM images of NCP (a) and $H_6P_2W_{18}O_{62}$/NCP (b).

under reduced pressure and finally the obtained crude product was purified through re-crystallization in EtOH : H_2O (3 : 1) as confirmed by an intense single spot in TLC. The pure products were specified based on the spectral data and determination of their melting points.

2.5. Calculation of pH_{pzc} (point of zero charge pH)

The pH_{pzc} is a point at which the surface acidic or basic functional groups no more chip in to the pH value of the solution.[16] Effect of surface modification with HPA on the acidity of nanozeolite was studied by calculating pH_{pzc} for HPA/NCP and NCP. The pH of a series of NaCl solutions (50 ml, 0.01 M) was adjusted to the value between 2 and 12 by addition of HCl (0.1 M) or NaOH (0.1 M) solutions in closed Erlenmeyer flasks. Then, pH of the solutions defined as the initial pHs (pH_I). Thereafter, 0.2 g of modified HPA/NCP (or unmodified NCP) was added and the final pH (pH_F) was measured after 48 h. Finally, the values of pH_F *vs.* pH_I and also pH_I *vs.* pH_I were plotted and the intersect of the lines provided the pH_{pzc}.[17]

3. Results and discussion

3.1. Characterization and physicochemical properties of the unmodified and modified NCP

CP is a natural material that belongs to the class of aluminosilicates containing exchangeable metal cations and water molecules in the internal crystalline cages. These types of zeolites contain open tetrahedral cages generating a system of channels which size is determined by the content of silicon. These cages are formed with a network of eight-member (channel B) and ten-member (channel A) rings, located in ab plane, and eight-member rings (channel C), located in *bc* plane (Fig. 1).

CP, as the most abundant natural zeolite, shows different shape and size selectivity, catalytic properties, ion exchange abilities, odor adsorbent behaviors, and molecular sieves properties.[19] Chemical and thermal stability of CP along with its pore system diameter are the most important parameters in studying conjunction of the HPA into the nanozeolite surface. Fortunately, the prepared NCP was suitably chemically and thermally stable in the presence of the utilized heteropolyacid. Since, the heterogeneous porous structure of CP consists of two types of primary (microporosity) and secondary (meso- and macro-porosity), therefore, heteropolyacids with the diameter ~10 Å, could be either encapsulated in the super cages of nanozeolite or supported in the secondary pore system.[20]

3.1.1. XRD and XRF patterns. Fig. 2 shows XRD patterns of NCP and HPA/NCP. With regards to the intensity ratio of major peak observed at 2θ about 22.5°, the crystalline structure of NCP was clearly attributed to the d_{004} reflection. Moreover, presence of broad lines in the XRD pattern of the prepared NCP particles established formation of nanoparticles during the ball milling process. The average crystallite size was calculated by *Debye–Sherrer*'s equation (eqn (1)), in which β denotes the excess width line at half-maximum of the diffraction peak in radians, θ is *Bragg* angle in degrees, and λ is the selected wavelength. By calculation, the average crystallite size of the prepared nanozeolite was attained ~40 nm. These results approved our method for the preparation of the nanosized CP.[21]

$$L = \frac{0.98\lambda}{\beta \cos(\theta)} \quad (1)$$

X-Ray fluorescence (XRF) revealed that SiO_2 (62.68%) and Al_2O_3 (9.57%) are the main constituents of NCP; whereas, P_2O_5 (0.03%) is the least component.[22] It has been established that the mole ratio of Si/Al would be a conventional distinction point between zeolites, CP has the ratio of Si/Al ≥ 4.0. The high mole ratio of silica/alumina (11.14) resulted in sufficient thermal and chemical stability, hydrophilic nature, and acidic strength of the nanozeolite to prepare acidic HPA/NCP catalyst.

3.1.2. SEM images. Morphology of the modified and unmodified NCP was studied by scanning electron microscopy (Fig. 3). The SEM image of the nanozeolite showed the layered structure of CP with layer thicknesses in nanometer range. The crystallites of the unloaded and loaded NCP with the heteropolyacid showed similar patterns; thus, loading process did not affect the crystallites structure. Although, there are some particles with micrometer dimension in the SEM pictures and lack of uniformity and wide range of particle dimensions, but the major particles had nanometer dimensions ranging from 30 to 70 nm. Loading of $H_6P_2W_{18}O_{62}$ led to enhancing particles size of the resultant nanocatalyst. Findings obtained by XRD and SEM approved that the selected method for the preparation

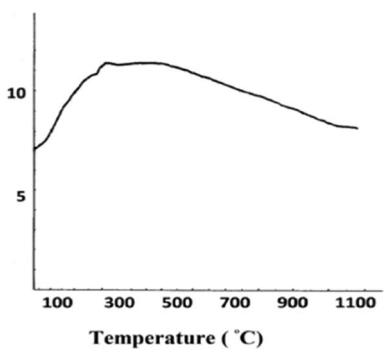

Fig. 4 Differential thermal analysis of NCP modified with $H_6P_2W_{18}O_{62}$.

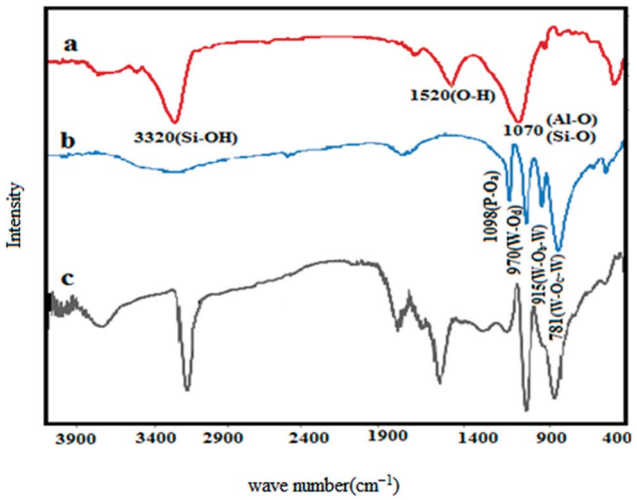

Fig. 5 FT-IR spectra of NCP (a), $H_6P_2W_{18}O_{62}$ (b), and $H_6P_2W_{18}O_{62}$/NCP (c).

of the nanosized CP was acceptable. It should be mentioned that mechanical production of zeolitic nanoparticles by means of planetary ball mills may also reduce CP crystallinity.

3.1.3. DTA analysis. Fig. 4 shows differential thermal analysis of $H_6P_2W_{18}O_{62}$/HPA. A continuous weight loss was occurred below 280 °C in the DTA analysis which was due to the removal of the physical adsorbed and coordinated water molecules. The modified NCP was stable up to 500 °C; however, the heteropolyacid structure started to degradation above this temperature.

3.1.4. FT-IR spectroscopy. The FT-IR spectroscopy was applied to characterize the composition of $H_6P_2W_{18}O_{62}$/NCP (Fig. 5). The nanozeolite showed three kinds of bands related to: (a) the internal broad Si–O(Si) and Si–O(Al) in the range of 1200–700 cm^{-1}, (b) zeolitic water molecules in the range of 2900–3500 cm^{-1}, (c) pseudo-lattice vibrations of structural units in the range of 500–700 cm^{-1}. A broad band about 3320 cm^{-1} is assigned to the symmetric and asymmetric stretching vibration modes of the surface silanol groups and stretching vibration modes of hydrogen-bonded water molecules adsorbed on the surface of nanozeolite. The Si–O–Si asymmetric stretching vibration overlapped with the stretching vibrations of Al–O–Si and Al–O and produced a broad band about 1070 cm^{-1}. The peak at about 1520 cm^{-1} is assigned to the O–H bending vibration of the adsorbed water molecules. Strong and broad bands in the region of stretching Si–O and Al–O bands and bending O–Si–O and O–Al–O vibrations confirmed high surface area of the prepared NCP.[23]

The structure of *Wells–Dawson* $H_6P_2W_{18}O_{62}$ involves two half units of a central PO_4 tetrahedron surrounded by nine WO_6 octahedra; therefore, four kinds of oxygen atoms appear in the FT-IR of HPA (Fig. 6). The first is due to P–O_a in which the oxygen atom is connected to the tungsten atom. The second is W–O_b–W oxygen bridges (corner-sharing oxygen bridges between different W_3O_{13} groups), the third is W–O_c–W oxygen bridges (edge-sharing oxygen bridge within W_3O_{13} groups), and the last is W–O_d terminal oxygen atoms. Therefore, four characteristic bands of $H_6P_2W_{18}O_{62}$ were appeared as ν_{as} (W–O_d, 970 cm^{-1}); ν_{as} (W–O_b–W, 915 cm^{-1}); ν_{as} (W–O_c–W, 781 cm^{-1}) and ν_{as} (P–O_a, 1098 cm^{-1}).[24]

3.1.5. UV-Vis spectroscopy. The UV-Vis spectrum of the *Wells–Dawson* heteropolyacid shows two types of ligand → metal charge-transfer bands originating from different oxygen atoms (Fig. 7). The highest energy absorption band below 250 nm (not shown) has been assigned to the O_d → W charge-transfer band due to the terminal oxygen atoms. Other weak and broad bands around 260 and 310 nm are characteristic bands of $H_6P_2W_{18}O_{62}$ and have been assigned to the O_b → W or O_c → W charge-transfer bands of the bridge-oxygen atoms.[25]

To find the minimum time required to load the maximum amount of $H_6P_2W_{18}O_{62}$ on NCP, further study was outlined through UV-Vis spectroscopy. Therefore, 0.1 g of NCP was suspended in 40 ml aqueous solution of HPA with the initial concentration of 2500 ppm. Then, the suspension was heated to 70 °C for different times ranging from 1 to 90 min. By comparison with the standard solutions, the heteropolyacid concentration had declined to 800 ppm after 90 min. This amount corresponds to 0.0311 mmol $g^{-1}$of $H_6P_2W_{18}O_{62}$ loaded on NCP. This result was confirmed by the amount obtained with MS-ICP which resulted in 0.0315 mmol $g^{-1}$of HPA.

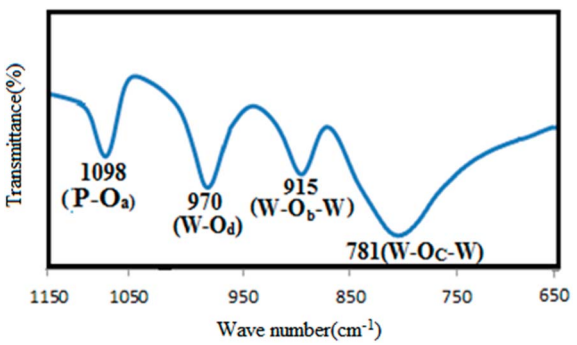

Fig. 6 Finger printing FT-IR bands of *Wells–Dawson* $H_6P_2W_{18}O_{62}$.

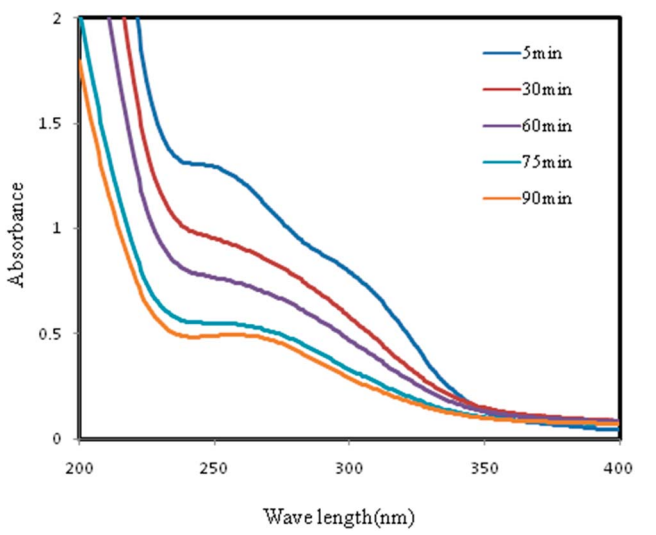

Fig. 7 Time dependence UV-Vis spectral changes after addition of $H_6P_2W_{18}O_{62}$ to NCP.

Table 1 The calculated and experimental parameters obtained for different initial weights of $H_6P_2W_{18}O_{62}$

Entry	Initial weight of HPA (g)	Amount of adsorbed HPA (μmol g^{-1} of NCP)	Weight of adsorbent (g)	C_e (g l^{-1})	Q_e (mg g^{-1})
1	0.02	7.7	0.5	0.070	34
2	0.05	19.4	0.5	0.190	85
3	0.10	32.9	0.5	0.700	144
4	0.20	35.9	0.5	1.790	157
5	0.30	37.5	0.5	2.950	164

3.1.6. Equilibrium studies. Different amounts of HPA were added to 40 ml deionized water in six separate conical flasks. To each flask was added the adsorbent NCP (0.5 g) with strong shaking. Then, the flasks were placed for almost 4 h with periodic shaking. Finally, the content of each flask was centrifuged and the separated solution was titrated against NaOH (0.01 N) in the presence of phenolphthalein with taking three readings in each case. The amount of the adsorbed HPA was calculated using eqn (2).

$$q_e = (C_0 - C_e)V/m \quad (2)$$

C_0 and C_e are initial and final concentrations of the heteropolyacid, respectively. m is the amount of adsorbent (g) and V is the volume (lit) of the reaction mixture (Table 1).

3.1.7. Adsorption isotherms. The extent of HPA adsorbed on NCP was calculated by the adsorption isotherm. Among several familiar isotherm equations, *Freundlich* and *Langmuir* isotherms are applied for this study and the experimental data were fitted with non-linearly. The *Langmuir* isotherm theory considers monolayer coverage of the adsorbate over a homogenous adsorbent surface and hints surface homogeneity of the adsorbent. Whereas, the *Freundlich* type adsorption isotherm is an indication of the surface heterogeneity of the adsorbent. The mass of HPA adsorbed on the solid adsorbent at various concentrations was calculated from the *Freundlich* eqn (3).[26]

$$q = KC_e^{1/n} \quad (3)$$

In which, K and n are *Freundlich* constants. Table 1 shows calculated and experimental values of q and C_e obtained at different HPA concentrations. K in this equation would be an indication of the adsorption capacity and $1/n$ would show the adsorption intensity. In general, as the K value increases, the adsorption capacity of the used adsorbent for a given adsorbate would be enhanced.

The *Langmuir* adsorption model[27] supposes that the maximum adsorption corresponds to a saturated monolayer of solute molecules on the adsorbent surface. The non-linear expression of *Langmuir* model is given by eqn (4):

$$q = abC_e/(1 + bC_e) \quad (4)$$

wherein, constants "a" and "b" are the *Langmuir* constants showing the capacity and energy of adsorption, respectively, and can be determined from the non-linear fitting. Therefore, "a" is the maximum amount of adsorbate per unit weight of sorbent to form a complete monolayer on the surface (mg g^{-1}) and corresponds to the free energy or net enthalpy of the adsorption. Moreover, "b" is a constant related to the energy of adsorption and indicates the stability of adsorbate–adsorbent composite. The applicability of *Langmuir* and *Freundlich* adsorption isotherms in the interaction of HPA with NCP is determined based on the correlation coefficient (R^2). The results summarized in Table 2 and Fig. 8, indicate that the reported experimental data correlates better with the *Langmuir* isotherm.

3.1.8. pH_{pzc} of the modified and unmodified NCPs. The pH_{PZC} for an inorganic material is the value at which the surface has a net neutral charge. It encompasses positive charge in solution with pH < pH_{PZC}; whereas, in a solution with pH > PH_{PZC} the negative charge would be developed at the surface of the mineral compound. These effects could be explained by deprotonation or protonation of aluminol Al–OH and silanol Si–OH groups in the framework of NCP.[28] The pH_{pzc} of the modified and unmodified NCPs were analyzed to evaluate effect of HPA loading on the acidity of NCP. Higher pH_{pzc} for the unmodified nanozeolite (pH_{pzc} 6.6) compared with HPA/NCP

Table 2 Values of *Langmuir* and *Freundlich* constants and regression coefficients

Freundlich constants		*Langmuir* constants	
K (mg g^{-1})	8.184	a (mg g^{-1})	200
$1/n$	0.397	b (g^{-1})	0.00398
R^2	0.872	R^2	0.980

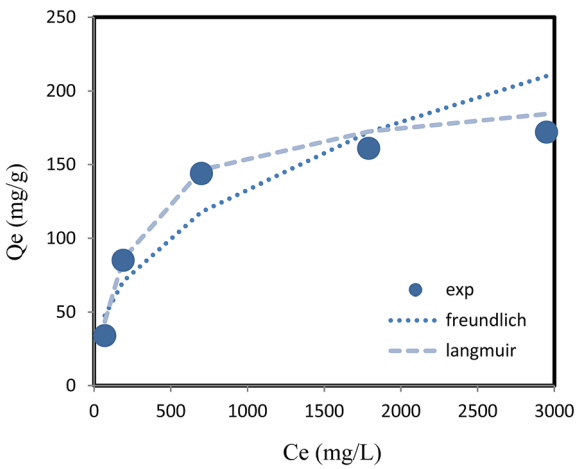

Fig. 8 The experimental and theoretical plots of HPA adsorption on NCP.

Table 3 Physicochemical properties of NCP and HPA/NCP

Characteristic	NCP	HPA/NCP
PH in water	8.7	8.1
PH_{pzc}[a]	6.6	6.0
The BET specific surface area ($m^2\ g^{-1}$)	125.5	91.597
Micropore specific surface area ($m^2\ g^{-1}$)	141.99	91.32
Micropore volume ($cm^3\ g^{-1}$)	0.0268	0.0183
Average pore diameter of BJH desorption (nm)	2.353	2.699

[a] Point of zero charge.

(pH_{pzc} 6), confirmed increment in the acidity of NCP after surface modification.

3.1.9. Pore characteristics of NCP before and after modification with HPA. Nitrogen adsorption isotherm, BET method, was applied to investigate changes in the specific surface area ($m^2\ g^{-1}$) of NCP after surface modification with HPA (Table 3). Micropore volumes were calculated by the *t*-plot method. Pore volumes were estimated from the amount of N_2 adsorbed at p/p_0 = 0–0.98. *Barret Joyner Halenda* (BJH) calculation was employed to estimate the pore-size distribution for NCP and HPA/NCP. Findings showed that the surface area of NCP was decreased after modification with HPA. Presumably, as HPA adsorbs on the external surface of HPA and pore opening takes place, the internal surface area of the NCP would be blocked and the micropore surface area decreases.[29]

3.2. Optimization of the reaction conditions

The best reaction conditions were attained by studying parameters affecting efficacy of the catalytic system. At first, a model reaction was conducted in the absence of catalyst which led to a very low yield (Table 4, entry 1). Then, effect of HPA loading on NCP was studied. As depicted in Table 4, 94% yield was attained in the presence of 15 mg HPA/NCP; whereas, only 13% was gained with the unmodified NCP. The results clearly approved the enforcing effect of HPA on the yield%. Effect of the amount of HPA was studied on the catalyst efficacy. The best yield achieved in the presence of 32.9–35.9 μmol HPA per g NCP.

Table 4 Screening effect of $H_6P_2W_{18}O_{62}$ loading on the catalytic activity of HPA/NCP[a]

Entry	Catalyst[b]	μmol HPA per g NCP	Time (h)	Yield (%)
1	None	—	24	<3
2	NCP (nanoclinoptilolite)	—	3	13
3	HPA ($H_6P_2W_{18}O_{62}$)	—	3	81
4	HPA/NCP	7.7	3	68
5	HPA/NCP	19.4	3	79
6	HPA/NCP	32.9	3	94
7	HPA/NCP	35.9	3	96
8	HPA/NCP	37.5	3	96

[a] Reaction conditions are described in the experimental section. [b] 15 mg of each catalyst was used.

Noteworthy, HPA/NCP containing a lower amount of HPA (7.7 μmol) was more effective than the situation utilizing 15 mg of the unmodified $H_6P_2W_{18}O_{62}$ (entry 3). The HPA loading was varied over the range 7.7–37.5 μmol HPA per g NCP. The conversion increased with enhancing catalyst loading, which was due to the proportional increase in the number of active sites. However, beyond a catalyst loading of 32.9 μmol HPA per g NCP, there was no significant improvement in the final yield% and reaction time as the available active sites exceeded that required; hence, all further experiments were carried out at 32.9 μmol HPA per g NCP.

3.3. Effect of catalyst amount on the cyclotrimerization reaction

The catalytic efficiency of various amounts of the heterogeneous HPA/NCP was investigated for the preparation of 1,3,5-triphenylbenzene (Table 5). At first, the nanosized HPA/NCP behaved better than the bulk modified clinoptilolite (HPA/CP). When 15 mg of the nanozeolite/HPA was employed, the desired product was gained in 90% yield within 2 h; whereas, only 58% yield was achieved during the same time with HPA/CP. Increasing concentration of HPA/CP from 5 to 15 mg enhanced yield% from 31 to 58% during the fixed time of 2 h. Noteworthy, no improvements were observed in yield% by enhancing either the reaction temperature or prolonging time.

In order to evaluate the appropriate catalyst amount, a model reaction was carried out by 5–20 mg of HPA/NCP. As is expected, yield% was grown by enhancing catalyst concentration. Moreover, only a little amount of HPA/NCP exhibited high catalytic activity in the desired transformation. Higher amounts of the catalyst (>20 mg) had not a significant effect on the yield%. Therefore, 15 mg of catalyst was found to be sufficient to push the reaction forward.

3.4. Surface modification of NCP by some heteropolyacids

Since, almost all heteropolyacids have low charge density on the surface and have no charge localization, the protons are very mobile, thus giving raise to extremely high *Brønsted* acidity. Nevertheless, catalytic activity of $H_6P_2W_{18}O_{62}$ was compared

Table 5 Effects of the size and amounts of the modified CP on the yield of the cyclotrimerization of acetophenone[a]

			Yield (%)	
Entry	Catalyst (mg)	Time (h)	HPA/CP	HPA/NCP
1	—	24	—	—
2	5	2	31	51
3	10	2	40	75
4	15	1	35	59
5	15	2	58	90
6	15	3	59	94
7	20	2	59	91

[a] Reaction conditions: acetophenone (1 mmol), at 100 °C, solvent free. Particles size of HPA/CP and HPA/NCP were ~70 μm and <70 nm, respectively.

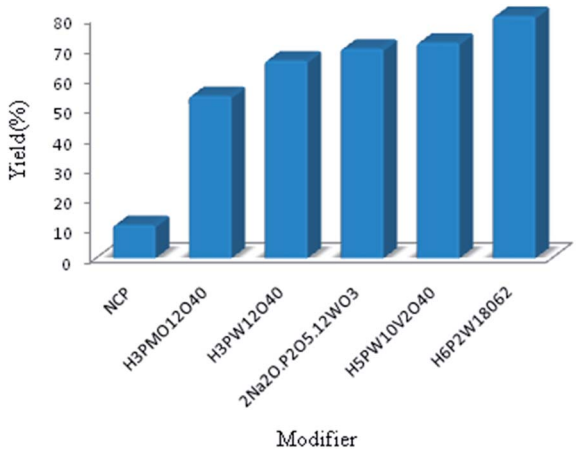

Fig. 9 Comparison of the catalytic activity of some heteropolyacids loaded on NCP. HPA/NCP (including ~35 μmol HPA/0.5 g NCP) was prepared as illustrated in Section 2.3. 0.01 g of each nanohybrid catalyst was used.

with other indicative familiar heteropolyacids in the preparation of 1,3,5-triphenylbenzene. All the introduced heteropolyacids are strong acids and behaved as good catalysts in the respective transformation (Fig. 9). However, *Wells–Dawson* poly tungstic acid $H_6P_2W_{18}O_{62}$ showed higher activity in the preparation of 1,3,5-triaryl benzene derivatives. Many factors such as acidity of the heteropolyacid, negative charge density smeared over oxygen atoms, structural composition and distortions, and absorption of the substrate molecule into the bulk of heteropolyacid would contribute to the catalytic efficiency of the heteropolyacids under the reaction conditions.

3.5. Effect of reaction temperature on the cyclotrimerization reaction catalyzed by HPA/NCP

Effect of temperature on the efficacy of the catalytic system was studied for the preparation of 1,3,5-triphenylbenzene under the optimized conditions (Fig. 10). The results showed that lower temperatures disfavored the reaction and only 13% yield was achieved after 180 min at room temperature; whereas, at 60 °C the reaction poorly proceeded and maximum conversion of 49% was reached after 3 h. The best result was gained at 100 °C and caused 94% yield at the same time. The product yield at 120 °C was slightly higher than that of 100 °C and further elevating temperature did not improve conversion. Therefore, we kept the reaction temperature as 100 °C.

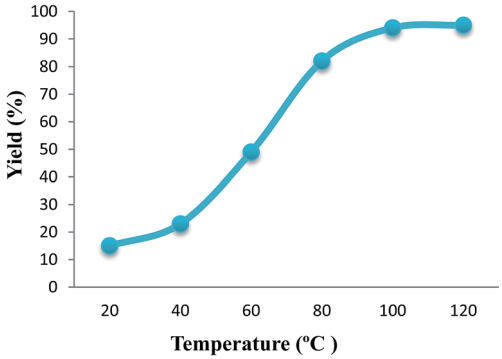

Fig. 10 Yield % as a function of reaction temperature in the cyclotrimerization of acetophenone.

3.6. Comparison of the catalytic efficiency of HPA/NCP with some reported catalysts for cyclotrimerization of acetophenone

Catalysts presented in Table 6 are Brønsted and/or Lewis acids and facilitate activation of the oxygen carbonyl group *via* coordination to the active site of acid catalyst. Moreover, hydrophilic characteristics of the used catalysts would help in adsorption of the generated water molecules and push the reaction forward. Considering these features, superiority of the presented heterogeneous catalyst was studied over some reported methodologies. The reaction of acetophenone for the synthesis of 1,3,5-triphenylbenzene was selected as a model reaction and the comparison was in terms of mol% of the catalysts, temperature, reaction time, and percentage yields. Obviously, the present new catalyst was superior over the reported catalysts considering the above variables. The present protocol utilized a very low amount of catalyst under solvent free condition. Obviously, the present protocol using a natural and simple catalyst was better than most of the conventional catalysts mentioned in Table 6.

3.7. Synthesis of different 1,3,5-triarylbenzenes catalyzed by HPA/NCP

Encouraged by the results, the capability of the present one pot, novel, and highly efficient methodology was assessed for the preparation of different 1,3,5-triphenylbenzene derivatives in the presence of HPA/NCP as a green, heterogeneous, and reusable natural catalyst under solvent-free conditions. For this purpose, a range of structurally diverse ketones such as methyl–

Table 6 Comparison of the catalytic activity of HPA/NCP with some reported catalysts towards cyclotrimerization of acetophenone

Entry	Catalyst	Catalyst (mol%)	Solvent	Time (h)	Temp. (°C)	Yield (%)	References
1	CAN	10	Free	10	130	>10	7*c*
2	$CuCl_2$	5	Free	10	130	38	7*c*
3	HCl	10	Ethanol	11	Reflux	45	7*b*
4	$SnCl_4$	10	Ethanol	24	Reflux	55	7*b*
5	PTSA	20	Free	3	130	60	6*b*
6	DBSA	10	Free	6	150	62	6*b*
7	HPA/NCP	15 mg	Free	3	100	94	This work

Table 7 Synthesis of different 1,3,5-triarylbenzenes catalyzed by HPA/NCP[a]

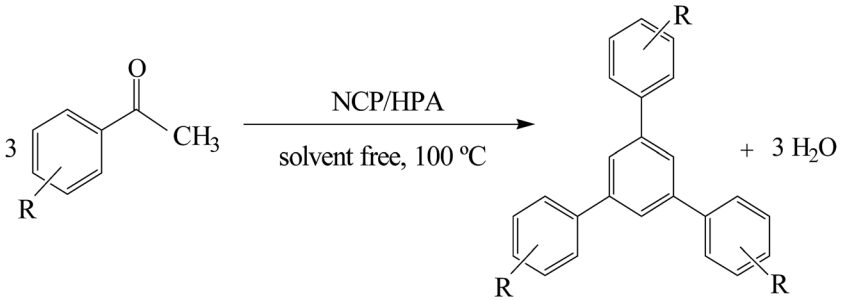

Entry	R	Time (h)	Yield (%)	Mp (°C)	Product	References
1	H	3	94	172–174	$(Ph)_3C_6H_3$	30
2	4-OMe	3	79	141–143	$(4\text{-}OMePh)_3C_6H_3$	30
3	4-Br	2.5	91	263–265	$(4\text{-}BrPh)_3C_6H_3$	31
4	$4\text{-}NO_2$	3	88	151–152	$(4\text{-}NO_2Ph)_3C_6H_3$	13*a*
5	4-Me	3	76	178–180	$(4\text{-}MePh)_3C_6H_3$	30
6	4-OH	3.5	77	237–239	$(4\text{-}OHPh)_3C_6H_3$	—
7	4-Cl	2.5	96	247–249	$(4\text{-}ClPh)_3C_6H_3$	30
8	4-F	2.5	98	237–239	$(4\text{-}FPh)_3C_6H_3$	31
9	Cyclohexanone	3.5	91	212–214	Dodecahydro-triphenylene	13*a*
10	Cyclopentanone	3.5	76	95–96	Trindane	13*a*

[a] Reaction conditions: substrate (1 mmol), 100 °C, 15 mg of HPA/NCP, solvent free. The structures of the products were established from their spectral properties and also by comparison with available literature data.

aryl ketones as well as cyclic ketones were condensed to furnish the corresponding products in good yield. As shown in Table 7, the acetophenones bearing electron-withdrawing substituents in the aromatic ring cyclotrimerized with higher rates and afforded the desired products in 88–98% yields. In contrast, the acetophenones having electron-donating substituents such as CH_3 and $-OCH_3$ at the aromatic ring reacted sluggishly and produced the corresponding 1,3,5-triarylbenzene derivatives in lower yields. In the case of acetophenones containing halogen at *para*-position of the aromatic ring, the yield of the cyclotrimerized product was significantly reduced, with decreasing electronegativity of the halogen. Therefore, yields of the triarylbenzenes varied with respect to the position of the substituents attached to acetophenone. The triple condensation reaction led to poor yields when *ortho*-CH_3 substituted acetophenone was used. Although, some previous reports declared no reaction with strong electron-withdrawing nitro group, the present system provided 88% yield after 3 h.[6b,7c] The obtained yields were found to be reproducible within ±3% variation.

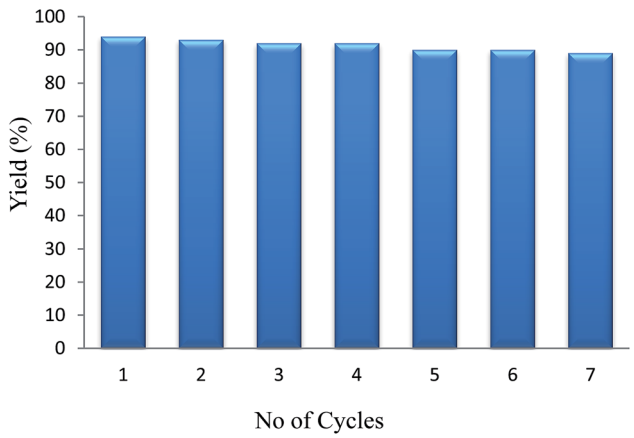

Fig. 11 Reusability of HPA/NCP in the cyclotrimerization of acetophenone.

3.8. Studying reusability of HPA/NCP in the cyclotrimerization of acetophenone

To investigate reusability of nanozeolite/HPA, it was easily separated from the reaction mixture by centrifuge and washed thoroughly with hot EtOH. Then, the catalyst was slowly dried in air and then was activated in a vacuum oven at 70 °C for 4 h. Finally, the recycled catalyst was reused for another condensation reaction. Findings revealed the same catalytic activity such as fresh catalyst, without any significant loss of activity (Fig. 11). Moreover, to ensure reproducibility of the transformation, repeated typical experiments were carried out under identical reaction conditions. The obtained yields were found to be reproducible within ±3% variation.

4. Conclusion

Immobilization of *Wells–Dawson* $H_6P_2W_{18}O_{62}$ on the external surface of the nanosized CP and generation of a new heterogeneous nanohybrid material, HPA/NCP, has been the target of this research. Then, the prepared catalyst was fully characterized and applied in the fast synthesis of different 1,3,5-triaryl

benzenes. This methodology offers the advantages of high yield, short reaction times, simple work-up, and green reaction conditions without formation of any by-products. Moreover, low cost as well as promoting the target transformation with appreciable yields are the main goals from both industrial and economic point of view. These advantages, in general, highlight this protocol as a useful and attractive methodology, among the methods reported in the literature, for the rapid synthesis of 1,3,5-triaryl benzenes. Finally, water was the only by-product in the whole process, which added to its attractiveness.

Acknowledgements

Partial financial support from the Research Councils of Hakim Sabzevari University is greatly appreciated.

References

1 M. J. Plater, M. Mckay and T. Jackson, *J. Chem. Soc., Perkin Trans. 1*, 2000, 2695.
2 T. Kadota, H. Kayeyama, F. Wakaya, K. Gamo and Y. Shirota, *Chem. Lett.*, 2004, **33**, 706.
3 R. Ghanbaripour, I. Mohammad poor-Baltork, M. Moghadam, A. R. Khosropour, S. Tangestaninejad and V. Mirkhani, *J. Iran. Chem. Soc.*, 2012, **9**, 791.
4 S. Zhang, Z. Xue, Y. Gao, S. Mao and Y. Wang, *Tetrahedron Lett.*, 2012, **53**, 2436.
5 (*a*) X. Y. Cao, X. H. Liu, X. H. Zhou, Y. Zhang, Y. Jiang, Y. Cao, Y. X. Cui and J. Pei, *J. Org. Chem.*, 2004, **69**, 6050; (*b*) E. J. Juarez-Perez, C. Vinas, F. Teixidor, R. Santillan, N. Farfan, A. Abreu, R. Yepez and R. Nunez, *Macromolecules*, 2010, **43**, 150.
6 (*a*) B. P. Dash, R. Satapathy, E. R. Gaillard, J. A. Maguire and N. S. Hosmane, *J. Am. Chem. Soc.*, 2010, **132**, 6578; (*b*) D. Prasad, A. Preetam and M. Nath, *C. R. Chimie*, 2013, **16**, 252.
7 (*a*) G. P. Zhang, R. H. Qiu, X. H. Xu, H. H. Zhou, Y. F. Kuang and S. H. Chen, *Synth. Commun.*, 2012, **42**, 858; (*b*) K. Phatangare, V. Padalkar, D. Mhatre, K. Patil and A. Chaskar, *Synth. Commun.*, 2009, **39**, 4117; (*c*) Y. Zhao, J. Li, C. Li, K. Yin, D. Ye and X. Jia, *Green Chem.*, 2010, **12**, 1370; (*d*) F. Ono, Y. Ishikura, Y. Tada, M. Endo and T. Sato, *Synlett*, 2008, **15**, 2365; (*e*) Z. Li, W. H. Sun, X. Jin and C. Shao, *Synlett*, 2001, 1947; (*f*) N. Iranpoor and B. Zeynizaded, *Synlett*, 1998, 1079.
8 F. Marme, G. Coudurier and J. C. Védrine, *Microporous Mesoporous Mater.*, 1998, **22**, 151.
9 M. E. Chimienti, L. R. Pizzio and C. V. Cáceres, *Appl. Catal., A*, 2001, **208**, 7.
10 R. Tayebee and B. Maleki, *J. Chem. Sci.*, 2013, **125**, 335.
11 (*a*) R. Tayebee, M. M. Amini, M. Ghadamgahia and M. Armaghan, *J. Mol. Catal. A: Chem.*, 2013, **366**, 266; (*b*) R. Tayebee, M. M. Amini, F. Nehzata, O. Sadeghi and M. Armaghan, *J. Mol. Catal. A: Chem.*, 2013, **366**, 140.
12 (*a*) M. Akgul, A. Karabakan, O. Acar and Y. Yurum, *Microporous Mesoporous Mater.*, 2006, **94**, 99; (*b*) G. S. P. Soylu, Z. Ozcelik and I. Boz, *Chem. Eng. J.*, 2010, **162**, 380; (*c*) M. Akgul and A. Karabakan, *Microporous Mesoporous Mater.*, 2010, **131**, 238; (*d*) M. Akgul, B. Ozyagcı and A. Karabakan, *J. Ind. Eng. Chem.*, 2013, **19**, 240.
13 (*a*) H. R. Safaei, M. Davoodi and M. Shekouhy, *Synth. Commun.*, 2013, **43**, 2178; (*b*) A. Kumar, M. Dixit, S. P. Singh, A. Goel, R. Raghunandan and P. R. Maulik, *Tetrahedron Lett.*, 2009, **50**, 4335; (*c*) X. Jing, F. Xu, Q. Zhu, X. Ren, C. Yan, L. Wang and J. Wang, *Synth. Commun.*, 2005, **35**, 3167.
14 G. P. Romanellia, D. M. Ruiza, H. P. Bideberripea, J. C. Autinob, G. T. Baronetti and H. J. Thomasa, *ARKIVOC*, 2007, **1**, 1.
15 S. M. Baghbanian, N. Rezaei and H. Tashakkorian, *Green Chem.*, 2013, **15**, 3446.
16 P. C. C. Faria, J. J. M. Orfao and M. F. R. Pereira, *Water Res.*, 2004, **38**, 2043.
17 A. Nezamzadeh-Ejhieh and H. Zabihi-Mobarakeh, *J. Ind. Eng. Chem.*, 2013, **20**, 1421.
18 A. Alberti, On the crystal structure of the zeolite heulandite, *Tschermaks Mineral. Petrogr. Mitt.*, 1972, **18**, 29.
19 (*a*) H. Lin, Q. Liu, Y. Dong, Y. Chen, H. Huo and S. Liu, *J. Mater. Sci. Res.*, 2013, **2**, 37; (*b*) O. Y. Saiapina, V. M. Pyeshkova, O. O. Soldatkin, V. G. Melnik, B. A. Kurç, A. Walcarius, S. V. Dzyadevych and N. Jaffrezic-Renault, *Mater. Sci. Eng., C*, 2011, **31**, 1490.
20 (*a*) N. Mansouri, N. Rikhtegar, H. Ahmad Panahi, F. Atabi and B. Karimi Shahraki, *Environ. Prot. Eng.*, 2013, **39**, 139; (*b*) Z. Olejniczak, B. Sulikowski, A. Kubacka and M. Gasior, *Top. Catal.*, 2000, **391**, 11.
21 (*a*) A. W. Burton, K. Ong, T. Rea and I. Y. Chan, *Microporous Mesoporous Mater.*, 2009, **117**, 75; (*b*) A. Nezamzadeh-Ejhieh and M. Shahanshahi, *J. Ind. Eng. Chem.*, 2013, **19**, 2026.
22 R. Tayebee, M. Jarrahi, B. Maleki, M. Kargar Razi, Z. B. Mokhtari and S. M. Baghbanian, *RSC Adv.*, 2015, **5**, 10869.
23 A. Nezamzadeh-Ejhieh and N. Moazzeni, *J. Ind. Eng. Chem.*, 2013, **19**, 1433.
24 R. Tayebee, F. Nehzata, E. Rezaei-Sereshta, F. Z. Mohammadi and E. Rafiee, *J. Mol. Catal. A: Chem.*, 2011, **351**, 154.
25 R. Tayebee, M. M. Amini, H. Rostamian and A. Aliakbari, *Dalton Trans.*, 2014, **43**, 1550.
26 E. Korngold, N. Belayev and L. Aronov, *Sep. Purif. Technol.*, 2003, **33**, 179.
27 J. Febrianto, A. Kosasih, J. Sunarso, Y. Ju, N. Indraswati and S. Ismadji, *J. Hazard. Mater.*, 2009, **162**, 616.
28 H. Guan, E. Bestland, C. Zhu, H. Zhu, D. Albertsdottir, J. Hutson, C. T. Simmons, M. Ginic-Markovic, X. Tao and A. V. Ellis, *J. Hazard. Mater.*, 2010, **183**, 616.
29 (*a*) R. Wei, J. Wang and G. Xiao, *Catal. Lett.*, 2009, **127**, 360; (*b*) Z. Fumin, W. Jun, Y. Chaoshu and R. Xiaoqian, *Sci. China, Ser. B: Chem.*, 2006, **49**, 140; (*c*) B. Sulikowski and R. Rachwalik, *Appl. Catal., A*, 2003, **256**, 173.
30 R. Ghanbaripour, I. Mohammadpoor-Baltork, M. Moghadam, A. Khosropour, S. Tangestaninejad and V. Mirkhani, *Polyhedron*, 2012, **31**, 721.
31 Q. Gao, F. Bao, X. Feng, Y. Pan, H. Wang and D. Li, *ARKIVOC*, 2013, **iii**, 49.

